

A Distributed Randle Circuit Model for Battery Abuse Simulations Using LS-DYNA[®]

Pierre L'Eplattenier¹, Iñaki Çaldichoury¹
James Marcicki², Alexander Bartlett², Xiao Guang Yang²,
Valentina Mejia², Min Zhu², Yijung Chen²

¹LSTC, Livermore, CA, USA

²Ford Research and Innovation Center, Dearborn, MI, USA

Abstract

Battery abuse research and modeling, Spatially-resolved battery modeling, Electro-thermal battery modeling.

A distributed Randle circuit model has been added to the electromagnetics (EM) module in LS-DYNA. This model implements so called "1st order Randle circuits" connecting two vis-à-vis nodes on the positive and negative current collectors which define a unit cell. These circuits consist of a state-of-charge dependent voltage source, internal resistance, and RC loop for damping effects. They empirically model the electrochemical processes occurring between the current collectors during charge or discharge, such as electrochemical reactions, lithium transport through the electrodes and separator, and electron transport to reaction sites within the electrodes. The EM solver and Randle circuits are coupled to give the potential, current density, and heating distribution in the unit cell and connected conductors. The heat generation is transferred to the thermal solver, which then feeds back to the temperature dependent Randle circuit parameters.

Several unit cells can be connected together either by a connecting mesh or by applying EM boundary conditions, hence forming a complete battery cell. Similarly, several cells can be coupled together to form a module. The main purpose of this model is the additional capability to model the electrical and thermal response to battery abuse scenarios, such as crash-induced crush. Depending on the local mechanical deformation occurring during a crush scenario, some of the Randle circuits can be replaced by a short resistance, hence triggering a local increase in the current flow and Joule heating which can lead to thermal runaway.

The distributed Randle model is described, as well as how to set up a typical case in LS-DYNA. The process for obtaining inputs to the Randle card is demonstrated. Basic benchmarks with experimental results are presented.

1-Introduction

Safety is an important functional requirement in the development of large-format, energy-dense, lithium-ion (Li-ion) batteries used in electrified vehicles. Computer aided engineering (CAE) tools that predict the response of a Li-ion battery pack to various abusive conditions can support analysis during the design phase and reduce the need for physical testing. In particular, simulations of the multiphysics response of external or internal short circuits can lead to optimized system designs for automotive crash scenarios.

In order to support virtual verification of a battery design, three-dimensional, transient simulations are required. These simulations should capture important aspects of battery physics, including their ability to store and deliver electrical power and the production of heat resulting from inefficient conversion of the stored electrochemical energy to electrical power. Furthermore, the interaction of battery cells with other system components including inert conductors and packaging materials should be captured. National laboratories and academic

research groups have developed similar models [1-3, 6-9] for computing solutions with realistic geometries, but there are limited commercially available options that support a large user base. Models that capture these types of physics can now be developed using LS-DYNA with the recent addition of several battery-related keywords.

This paper documents the model assumptions, structure, and initial benchmarking comparisons with experiments. First, a background description of battery phenomenological models is discussed along with data-driven parameterization techniques. Then, the implementation of the spatially-resolved, transient model in LS-DYNA is presented. Finally, the model is compared with experimental data for nominal cycling conditions such as pulse power and capacity testing at several current rates, states-of-charge, and temperatures, to demonstrate its effectiveness.

2-Electrothermal Model Development

In this section, the keywords that define an electrothermal battery model are described. The experimental data and the process used to estimate model parameters is reviewed. Methods for coupling the battery keywords to the thermal and mechanical solvers are discussed, and finally the post-processing capabilities implemented in LS-PrePost[®] are demonstrated.

2-1 Lumped Randle model

Phenomenological models are often used to represent battery behaviors. The most common ones are equivalent circuit models [4-5]. They are simple but capable of capturing battery dynamics for different operating conditions.

Amongst such equivalent circuits are the so called “Randle” circuit models. They are electrical circuits composed of an ideal voltage source, an internal resistance and n parallel RC circuits, n being the order of the model. The RC circuits give the damping effects that are usually present in the measured voltages. The circuit elements are not constant, but functions of the state of charge (SOC), temperature, and current direction. These dependencies give a broad range of validity to the model, and it was decided that a 1st order Randle circuit was a good compromise between accuracy and the somewhat cumbersome parameter identification of the circuit elements. A 1st order Randle circuit is shown in **Fig. 1**.

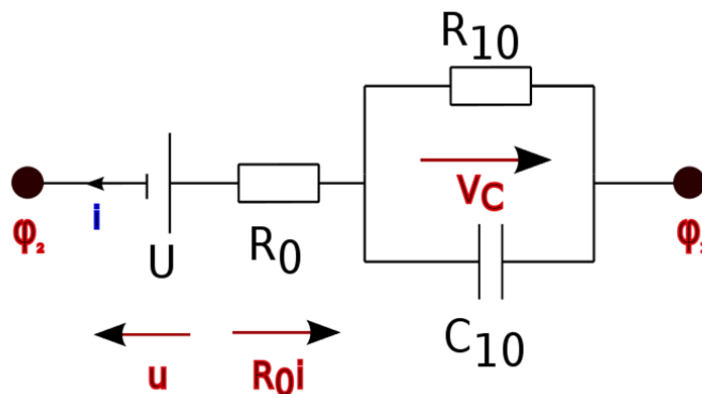


Figure 1: A 1st order Randle circuit.

The total voltage across the electrodes is split between the open-circuit voltage (OCV) u , the product of the current and the internal resistance $r_0 i$, and the dynamic overpotential v_c , which satisfies, after slightly transforming the circuit equations:

$$\frac{dv_c}{dt} = \frac{i}{c_{10}} - \frac{v_c}{r_{10}c_{10}} \quad (1)$$

The OCV of a cell is usually defined by a SOC, representing how much the battery is charged relative to its total capacity. A cell is fully charged (SOC=100%) when its charge q is equal to its capacity Q usually defined in Ah. If we write q in Coulombs, the relation between q and SOC thus is:

$$q = Q \times 3600 \times \frac{SOC}{100} \quad (2)$$

or:

$$q = \frac{Q}{c_Q} \times SOC \quad (3)$$

where $c_Q = \frac{1}{36}$ is the SOC conversion factor (%/s).

The open-circuit voltage u is generally a function of SOC. **Fig. 2** shows such a typical function, though in terms of actual capacity rather than normalized to SOC. One can see that down to 40%, the dependency is quasi linear, and hence the cell behaves like a capacitor. In fact, on this particular example, the linear fit of u vs SOC written in terms of charge q in Coulomb reads:

$$u \approx u_0 + \frac{1}{C}(q - q_0) \quad (4)$$

With $u_0 = 4.15V$, $q_0 = 72000C$ and an equivalent capacity $C = 1.3 \times 10^5 F$, which is a huge value in the world of capacitors, but which makes sense since a cell is able to store a lot of energy. From **Eq. 3** and the fact that $i = \frac{dq}{dt}$, SOC satisfies:

$$SOC(t) = SOC(t_0) - \frac{c_Q}{Q} \int_{t_0}^t i(t) dt \quad (5)$$

And usually, r_0 , r_{10} and c_{10} depend on SOC, the temperature, and the direction of the current (discharge if > 0 , charge if $i < 0$). Various characterization experiments are used to establish these dependencies for a given cell type. For the parameterization process, a 0-D circuit is assumed when comparing the model prediction to experiments, rather than the full, computationally expensive distributed circuit model. This allows for optimization of the parameters in a reasonable time. Then, the optimized parameter relationships obtained using the 0-D model are transferred to the distributed model, after they are appropriately scaled based on the number of nodes and unit cells contained in the complete cell.

2-1-1 Open Circuit Voltage

To establish the open circuit voltage (OCV) as a function of SOC, C/10 capacity tests were conducted. This means that the cell is discharged with a constant current, at a rate that discharges the rated capacity in a time of ten hours. The OCV is taken as the average of the charge and discharge curves at 25°C, and the low C/10 rate is used to approximate the open circuit (no-load) condition. OCVs for each cell type are shown **Fig. 2**.

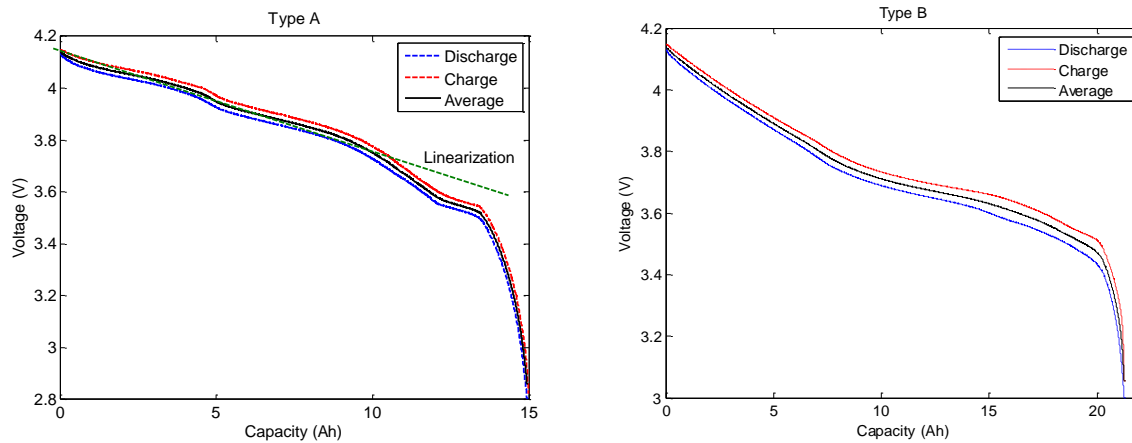


Figure 2: C/10 capacity tests for each cell type. The OCV is taken as the average between charge and discharge curves. The Type A plot also shows the linearization discussed in Section 2-1.

2-1-2 Resistance and Capacitance Parameters

The Hybrid Pulse Power Characterization (HPPC) test (shown in **Fig. 3**) consists of a series of charge and discharge pulses, at different discrete SOCs and a given ambient temperature, in order to parameterize the resistor and capacitor elements as functions of SOC, temperature, and current direction. The HPPC test applies 10 s charge and discharge pulses at SOCs from 90% to 10%, in increments of 10%. Model parameters are defined at each discrete SOC level, and defined separately for charge and discharge. Temperature dependencies are then established by repetition of the HPPC test at different operating temperatures, in this case 25°C, 40°C, and 50°C.

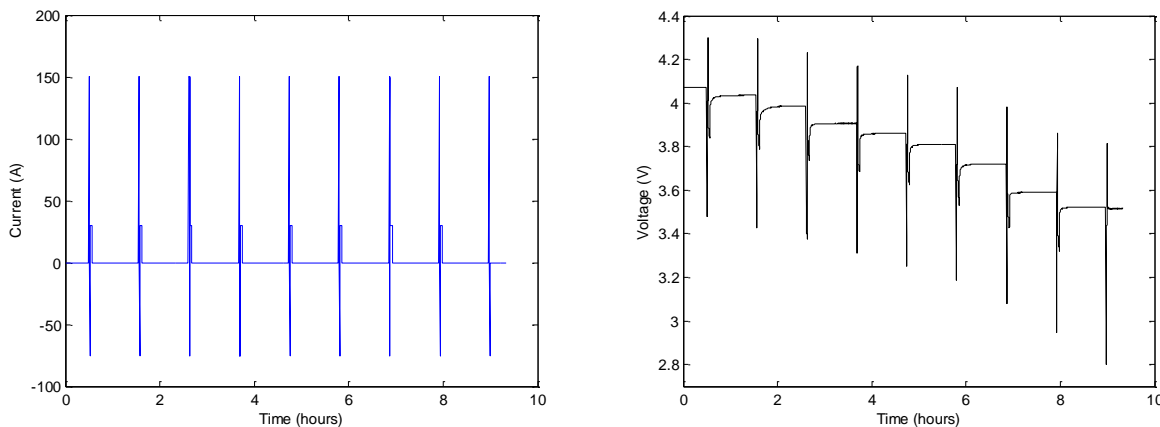


Figure 3: Example HPPC test, for a type A cell at 25°C.

The series r_0 parameter captures the initial Ohmic voltage jump following a step change in current. Physically, this represents the near-instantaneous sources of overpotential, including the electrical resistance between the electrode active material and battery tabs, reaction kinetics, and ionic conductivity in the electrolyte. The r_0 parameter is quantified for each charge and discharge pulse simply by recording the voltage jump immediately following a current pulse, and using Ohm's law, i.e. $r_0 = \frac{\Delta V}{\Delta I}$. The parallel r_{10} and c_{10} pair captures the longer term, relaxation behavior following application or removal of current. This behavior is the result of lithium concentration gradients (and resulting overpotentials) that form in both the solid and liquid phase as the applied current is sustained. The r_{10} and c_{10} parameters are fit using a linear least squares algorithm [10] to the 10 s pulses at each SOC level.

The identification of r_0 , r_{10} , and c_{10} is repeated for HPPC tests at each temperature, establishing a 2-D lookup table between SOC, temperature, and the parameter value. Parameters are extrapolated to temperatures outside of the range tested by assuming an Arrhenius dependence of the parameters on temperature. In addition, since discharge or charge pulses cannot be applied at 0% or 100% SOC, respectively, parameter values for these extreme SOCs are tuned manually. Following the parameterization of R_0 , R_{10} , and c_{10} as functions of SOC, current direction and temperature using the 0-D model, the parameter relationships for the distributed model are appropriately scaled based on the number of unit cells and number of nodes within a unit cell in order to evaluate the Randle circuit parameters at each node based on the local SOC, current direction, and temperature.

2-1-3 SOC Shift

At sustained high rate discharges, which are particularly relevant to external short and overcharge scenarios, diffusion limitations occur, and the model was amended to take them into account by adding a SOCshift term, which is added to SOC to evaluate the voltage source u and the internal resistance r_0 as $u(\text{SOC} + \text{SOCshift})$ and $r_0(\text{SOC} + \text{SOCshift}, T)$. The SOCshift is a damped term which satisfies **Eq. 6** :

$$\frac{d(\text{SOCshift})}{dt} + \frac{\text{SOCshift}}{\tau} = \frac{f(i)}{\tau} \quad (6)$$

where τ is the damping factor and $f(i)$ a function of the Randle current. In order to parameterize the SOC shift, particularly relevant to high rate, sustained discharges, multi-rate capacity tests were conducted at C-rates of 1, 2, 3, 4, 5, and 10C, at ambient temperatures of 25°C and 40°C.

In **Eq. 6**, there are two tunable parameters, τ and $f(I, T)$, that affect the SOC shift dynamics. These parameters can be tuned to match experimental data. Once again, a 0-D model is used to optimize the SOC shift parameters in order to reduce the computational effort. Note that τ is assumed to be constant and independent of current and temperature. Therefore $f(I, T)$ is optimized for each capacity test (at a given I and T) and a constant τ is optimized over all capacity tests. Matlab's `fminsearch` command is used to accomplish this, with the objective

function for a given capacity test i defined as: $J_i = w_1 \sqrt{\frac{1}{N_i} \sum_k (V_{k,i} - \hat{V}_{k,i})^2} + w_2 (|V -$

$\widehat{V}|_{\text{at } V_{\text{low}}}_i$), where $V_{k,i}$ is the measured voltage at time k , $\widehat{V}_{k,i}$ is the model predicted voltage at time k , N_i is the total number of data points in capacity test i , and the term $(|V - \widehat{V}|_{\text{at } V_{\text{low}}}_i)$ is the voltage error at the end of the discharge (lower voltage limit). This ensures that emphasis is placed not just on minimizing the total root-mean-square error (RMSE) throughout the test, but also on matching the voltage at the lower limit and therefore matching the capacity reduction for a given rate and temperature. Weights w_1 and w_2 can be given to each term to the RSME and lower limit voltage error terms, to emphasize one criteria more than the other.

Since τ is defined as a constant for a given cell type, while $f(I, T)$ is allowed to vary with rate and temperature, a two level optimization routine is utilized. For each guess of τ , the optimal $f(I, T)$ that minimizes J_i for each capacity test is found. Then the guess of τ is iterated until the total sum of all J_i s over all operating conditions is minimized. The optimal τ was determined to be 200 s for both type A and B cells.

2-2 Distributed Randle Model

The idea of the distributed Randle model is to use a certain number of Randle circuits between corresponding nodes on the two current collectors of a unit cell, as demonstrated in **Fig. 4**. These Randle circuits model the electrochemistry that happens in the electrodes and separator between the current collectors. The EM solver can then solve for the EM fields in the current collectors, and the connections between them. In fact, the events occurring in a battery crush are in general sufficiently slow so that the inductive effects can be neglected. Hence the EM resistive [11] solver is perfectly suitable for such studies.

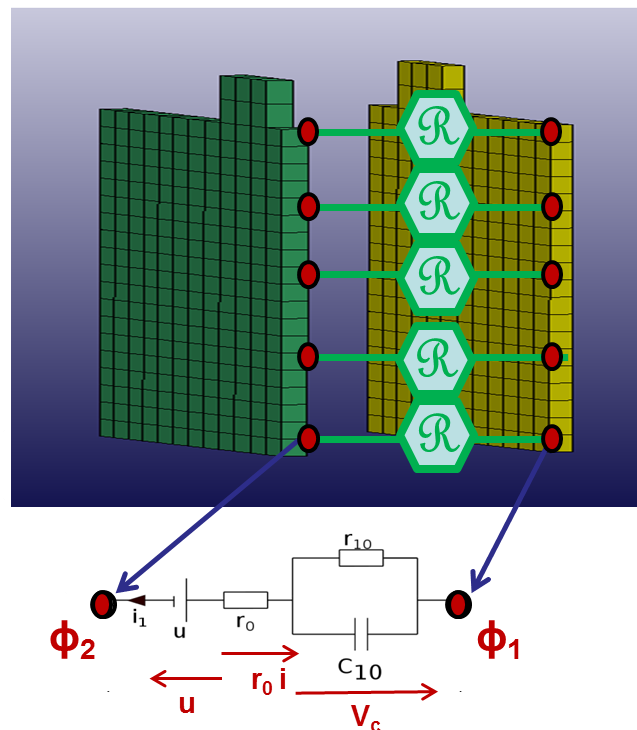


Figure 4: Schematic for a distributed Randle circuit between 2 current collectors. In the picture, each \mathcal{R} represents a Randle circuit

Some additions had to be made to the standard EM resistive solver to account for the Randle circuits. The standard EM resistive solver solves a Laplacian equation on the scalar potential at the nodes φ [11]:

$$S_0(\sigma)\varphi = 0 \quad (7)$$

where $S_0(\sigma)$ is the Laplace operator which depends on the local element conductivity σ , along with adequate boundary conditions (generally, the value of the potential is set at certain nodes). From the scalar potential φ , the current density \vec{j} is computed as:

$$\vec{j} = \vec{\nabla}\varphi \quad (8)$$

And the joule heating power as:

$$P_j = \frac{j^2}{\sigma} \quad (9)$$

The extra Randle circuits add a RHS to **Eq. 7**, to take into account the potential drop between the opposite nodes on the current collectors:

$$\varphi_2 - \varphi_1 = u - r_0 i - v_c \quad (10)$$

In fact, for numerical stability reasons, it was decided to include the $r_0 i$ part of this RHS into the Laplacian operator $S_0(\sigma)$. The modified system thus reads:

$$((S_0(\sigma) + D(r_0))\varphi = b \quad (11)$$

Where:

$$D(r_0) = \frac{1}{r_0} \text{ at } (N_1, N_1) \text{ and } (N_2, N_2) \quad (12)$$

$$D(r_0) = -\frac{1}{r_0} \text{ at } (N_1, N_2) \text{ and } (N_2, N_1) \quad (13)$$

$$D(r_0) = 0 \text{ elsewhere} \quad (14)$$

And

$$b = \frac{1}{r_0}(u - v_c) \text{ at } N_1 \quad (15)$$

$$b = -\frac{1}{r_0}(u - v_c) \text{ at } N_2 \quad (16)$$

$$b = 0 \text{ elsewhere} \quad (17)$$

Once system (11) is solved, the current i flowing in the different Randle circuits can be computed by:

$$i = S_0(\sigma)(N_1) = -S_0(\sigma)(N_2) \quad (18)$$

which allows actualization of v_c and SOC as (see equations 1 and 5)

$$v_c(t + dt) = v_c(t) + dt \left(\frac{i}{c_{10}} - \frac{v_c(t)}{r_{10}c_{10}} \right) \quad (19)$$

$$SOC(t + dt) = SOC(t) - dt \frac{c_q}{Q} \quad (20)$$

2-2 Connection with external circuits

Two new cards have been added in connection with the Randle circuit,

- a- *EM_ISOPOTENTIAL constraining a set of nodes to be at the same potential. This is a convenient way to connect the positive and negative current collectors of different unit cells or cells together without having to provide a mesh for such connections, which can be delicate. This is illustrated in **Fig. 5**.

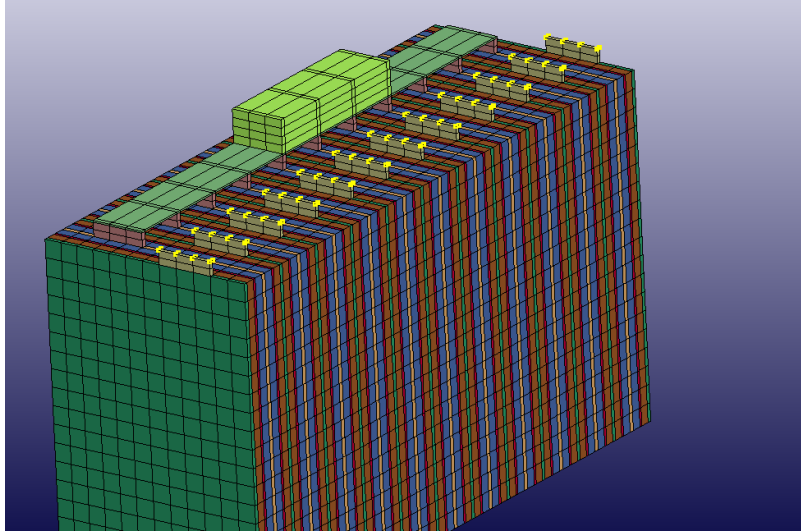


*Figure 5: A cell with the anode current collectors connected with meshed connectors and the cathode ones with a node set and the use of *EM_ISOPOTENTIAL. Note that the cell thickness was increased for viewing purposes.*

- b- *EM_ISOPOTENTIAL_CONNECT

This card, shown in **Fig. 6**, is for connecting two isopotentials by a short circuit, a time dependent resistance, voltage source or current source, to easily set up the cell in the condition it is tested, charge, discharge, HPPC tests, external shorts and so forth.

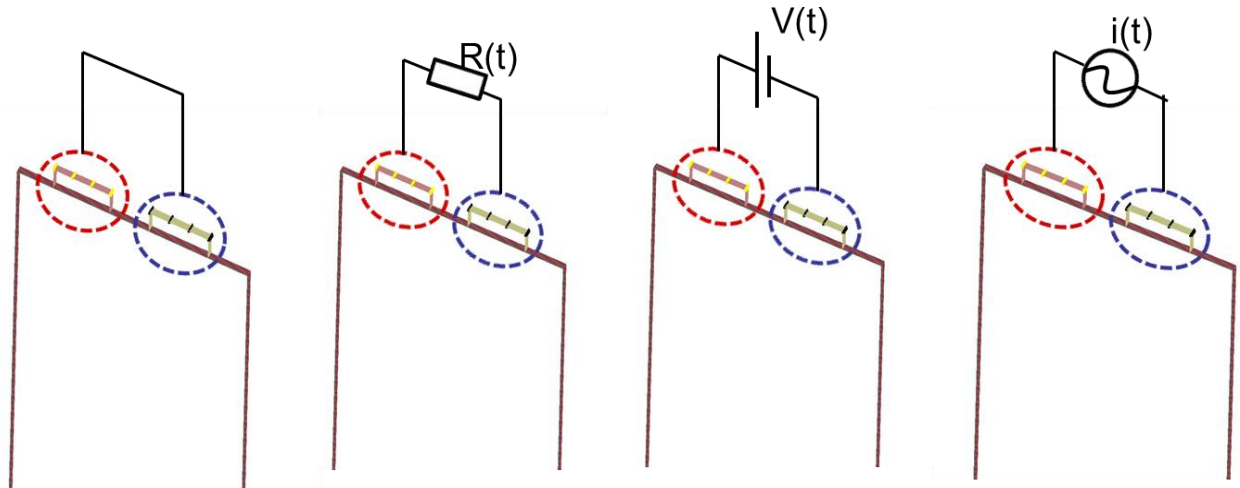


Figure 6: The different connections handled by the *EM_ISOPOTENTIAL_CONNECT card

2-3 Thermal Coupling

As we showed previously, for the EM solver, the only parts that need to be meshed are the current collectors. The electrochemistry happening in the anode, cathode and separator is taken into account by the Randle circuits. For the thermal, though, it may be important to add these layers, at least so that their thermal capacity is taken into account, since they represent a non-negligible part of the total mass of the system. If an EM/thermal simulation is performed, the anode, cathode and separator should thus be added to the model. In this case, the joule heating coming from the internal resistance r_0 of the Randle circuits is locally added to the thermal solver in the separator (a unit cell is so thin that it instantaneously diffuses to the anode, cathode, and current collectors). The local temperature from the thermal solver is used to evaluate the r_0 , r_{10} and c_{10} of each Randle circuit.

Another term, SOC-dependent reversible heat, can also be locally added to the thermal solver. The heating power is given by:

$$P_R = iT \frac{dU}{dT} \quad (21)$$

Where i is the Randle current, T the temperature and $\frac{dU}{dT}$ depends on the SOC.

Fig. 7 gives an overview of the EM/thermal coupling.

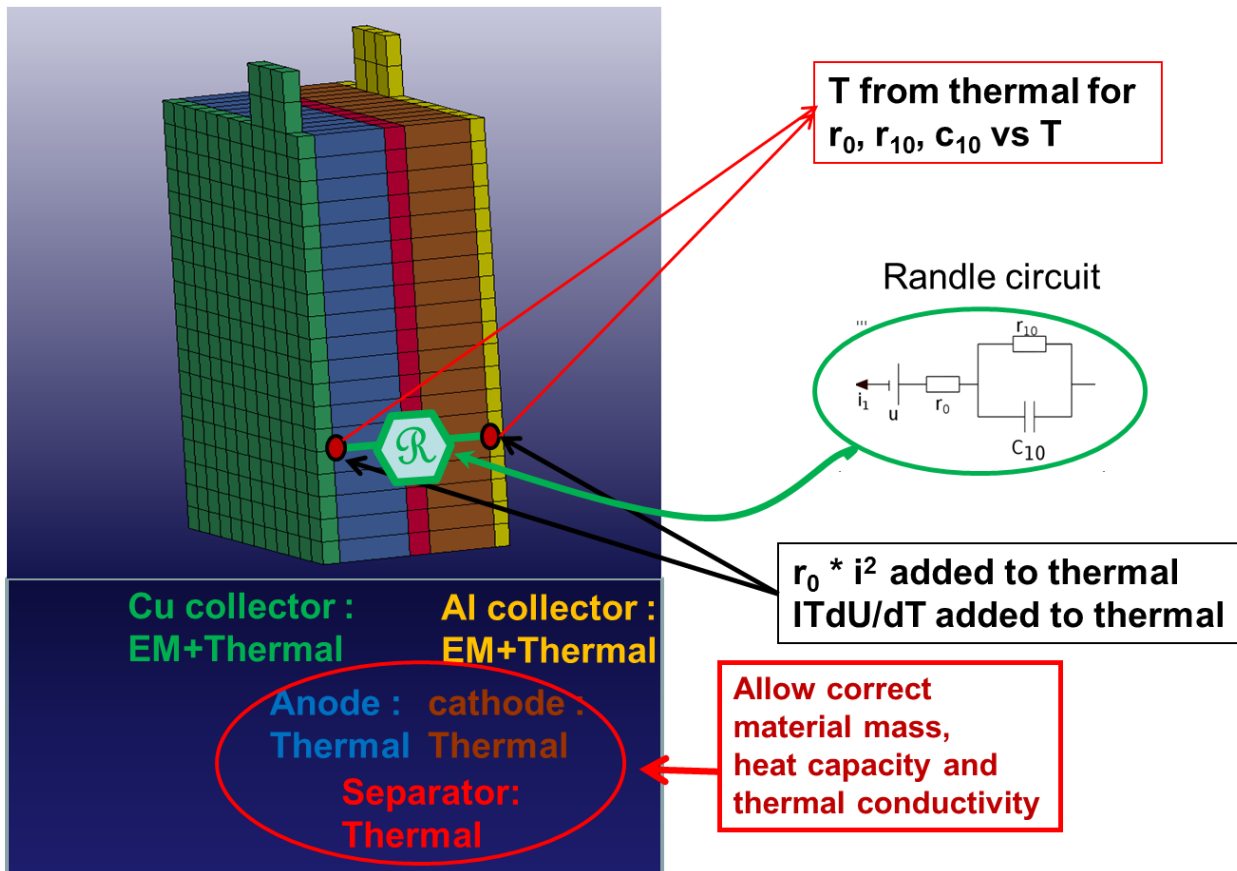


Figure 7: Overview of the EM/thermal coupling

2-4-1 Energy Balance

The representation of the electrochemical processes in terms of Randle circuits (**Fig. 1**) gives an easy computation of the different parts of the energy. The total energy available in a fully charged cell reads:

$$E_{available} = \int u(t)i(t)dt = \int udq = \frac{Q}{C_Q} \int u(SOC)dSOC \tag{22}$$

Which depends only on the u(SOC) curve. The energy delivered by u reads :

$$E_u = \int u(t)i(t)dt \tag{23}$$

The energy actually delivered to the load reads:

$$E_Q = \int u_{load}(t)i_{load}(t)dt \tag{24}$$

The energy “lost” in joule heating in the internal resistance

$$E_j = \int R_0(t) i^2(t) dt \quad (25)$$

In all the equations above, the integrals are added over all the Randle circuits participating in the cell.

Fig. 8 shows the different energy contributions during a typical battery discharge.

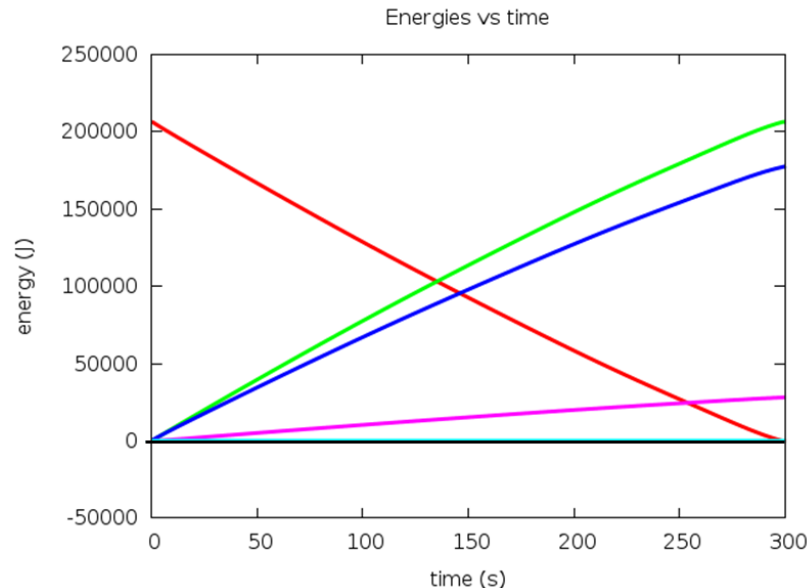


Figure 8: Energy balance in a typical battery discharge: $E_{available}$ (red), E_u (green), E_Q (blue) and E_j (pink).

2-4-2 Thermal Parameter Identification

To identify the cell thermal parameters such as heat capacity and heat transfer coefficient, an experiment was conducted on the Type A and Type B cells described in section 3.1. A known heat input was applied to a single battery cell and the resulting surface temperatures were measured at different locations. The ambient temperature variation near the cell due to convection was also recorded. A 0-D model was applied to this experimental data and preliminary, bulk cell heat capacity and heat transfer coefficients were identified using LS-OPT[®].

Using these bulk cell properties, a LS-DYNA thermal (*CONTROL_SOLUTION, SOLN 1), transient (*CONTROL_THERMAL_SOLVER, ATYPE 1), MPP (*CONTROL_THERMAL_SOLVER, SOLVER 11) model was created to simulate the distributed thermal behavior of the cell. A heat generation load (*LOAD_HEAT_GENERATION_SET) was applied to the model on a portion of the top and bottom surface of the cell, replicating the experimental film heater time series. A convection set boundary condition (*BOUNDARY_CONVECTION_SET) with the bulk heat transfer coefficient calculated from the experimental data was also applied to the model. An initial ambient temperature of 25°C, a time step of 1s and an end time of 6000s were also applied to the model. The cell materials were treated as a bulk material, using the same material properties for all the cell components. To create the portion of the top and bottom surfaces where the heat

generation load was applied a *SET_SOLID containing the elements located where the experimental heater was placed was generated. For the convection boundary, a *SET_SEGMENT comprising of the top and bottom surfaces was used. The heat input versus time was defined as a curve (*DEFINE_CURVE) and this curve was applied to the LOAD_HEAT_GENERATION_SET.

The resulting surface temperatures of the model were compared to the experimental surface temperatures, and a RMS error was calculated. The preliminary heat capacity and heat transfer coefficient identified from the 0-D model were further tuned to obtain a better fit based on the RMS error calculation. These set of values were chosen based on the initial 0-D model found values. **Fig. 9** shows the obtained best fit, with RMS errors of 0.37°C and 0.78°C for Type A and Type B cells, respectively.

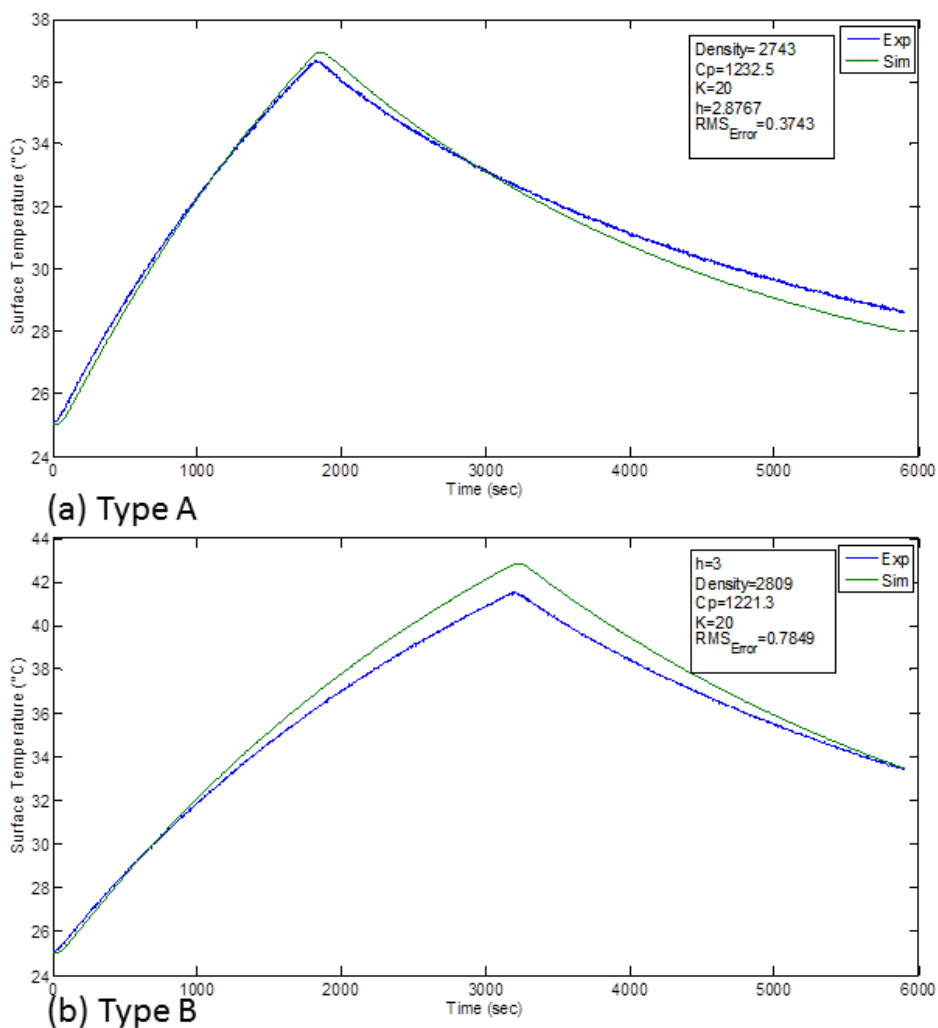


Figure 9: Comparison of experimental versus model simulated results with optimal heat capacity and heat transfer coefficient values for (a) Type A cell and (b) Type B cell.

2-4 Internal short

A major advantage of the distributed Randle model is the capability to locally switch from a Randle circuit, representing a battery in normal use, to another circuit, for instance a resistance in areas where an internal short circuit is detected. The criteria for the detection of a short in an area could be based on a distance threshold between the current collectors, the local erosion of the separator and so forth. The value of the short resistance r_s , is of course critical and should be determined in combination with experimental data. **Fig. 10** illustrates this process.

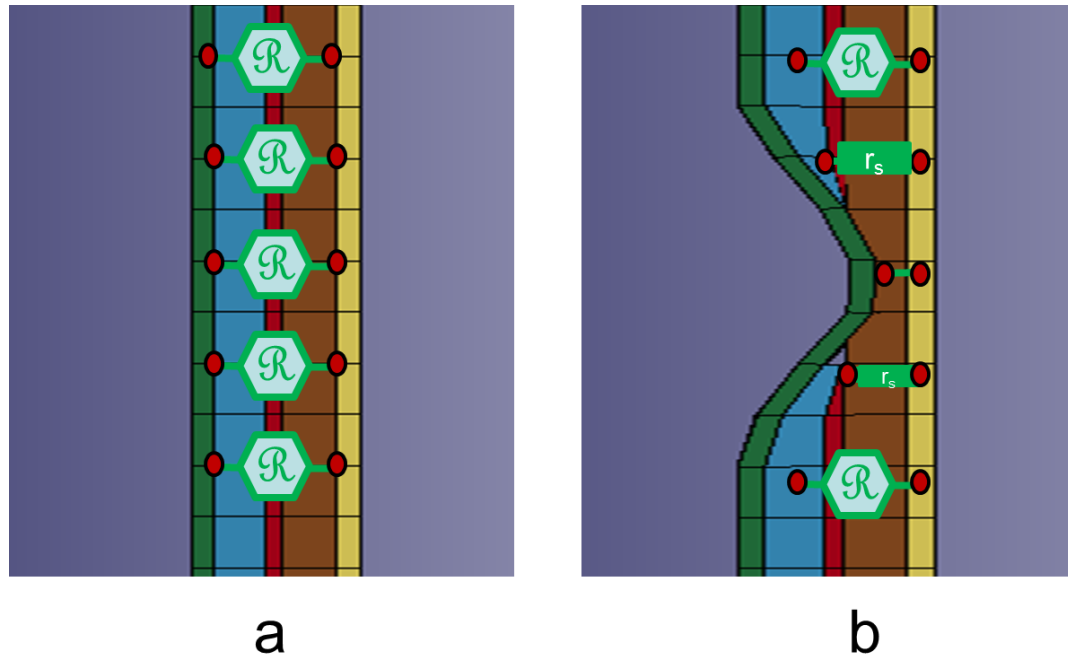


Figure 10: Illustration of the switch from Randle circuits (a) to resistances (b) when an internal short happens.

2-5 LSPREPOST

On top of the already available EM d3plot output (scalar potential, current density, Joule heating and so forth), displayed on the conductors (i.e. the current collectors and different connectors), the Randle circuit parameters, r_0 , r_{10} , c_{10} , SOC , i , u , v , v_c , P_{joule} , $P \frac{du}{dT}$, can be visualized in Lsprepost. It was decided to show them on the separator since each node on the separator belongs to a unique unit cell hence a unique Randle circuit.

Fig. 11 shows an example of fringe components for a unit cell during a discharge.

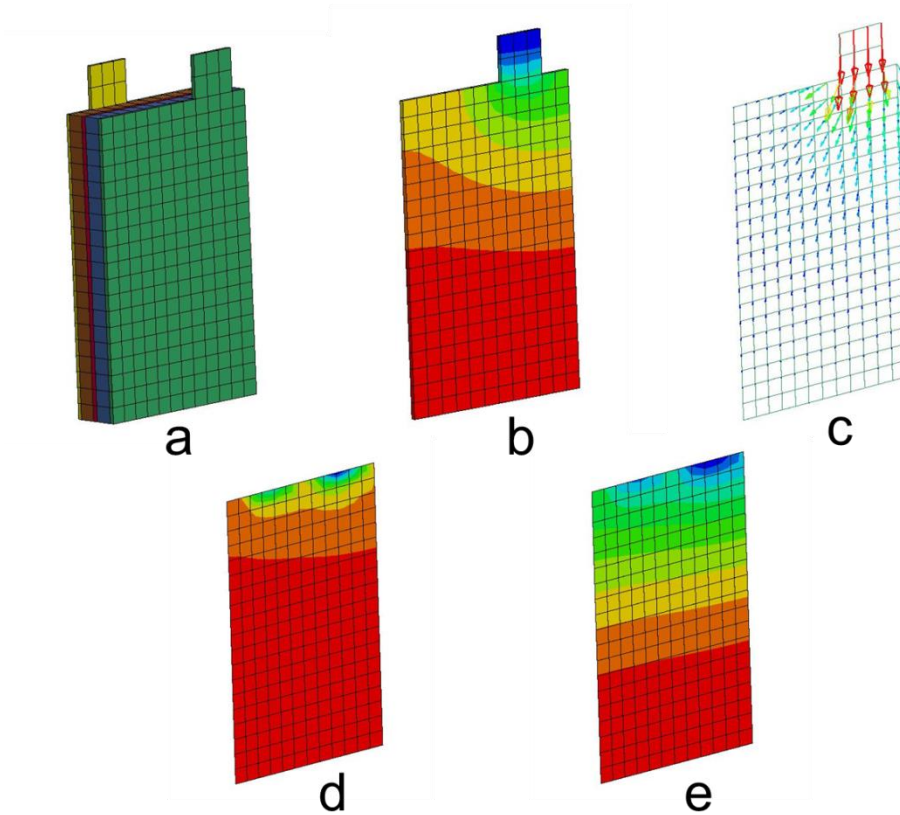


Figure 11: Example of d3plot output on a unit cell (a), where the thickness was zoomed, with the scalar potential on a current collector (b), current density on the current collector (c), r_0 on the separator plane (d) and SOC on the separator plane (e).

3-Benchmarking with Experimental Results

The benchmarking procedure consists of building meshes for two cell types, subjecting the cells to various electrical cycling experiments, and attempting to match the experimental results with simulations. The cycling experiments proceed from quick tests designed to test the transient response to longer tests that further stress the coupling between the thermal and electrochemical behavior of the cells.

3.1 Cell Descriptions

The cells used for experimental benchmarking are summarized in **Tab. 1**. The cells are meshed as five distinct parts representing the separator, the negative electrode active material, the negative electrode current collector, the positive electrode active material, and the positive electrode current collector. Each part contains multiple layers representing the unit cells throughout the cell thickness, and each mesh consists entirely of solid elements with 5 mm edge length, and one element through the thickness of each component.

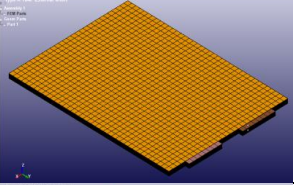
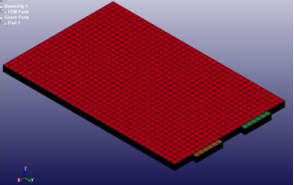
Image	Type	Cathode Chemistry	Dimensions	Number of Elements
	A	NMC/LMO	195 mm x 145 mm	151k
	B	NMC	195 mm x 125 mm	153k

Table 1: Cell characteristics for experimental benchmarking study.

3.2 HPPC Validation

The distributed model is able to accurately predict the voltage dynamics of the HPPC test, as shown in **Fig. 12** (at 25°C) and summarized in **Fig. 13**. Note that this validation utilizes an HPPC test with a different current pulse magnitude from the one used to establish the parameters, demonstrating some robustness to current inputs.

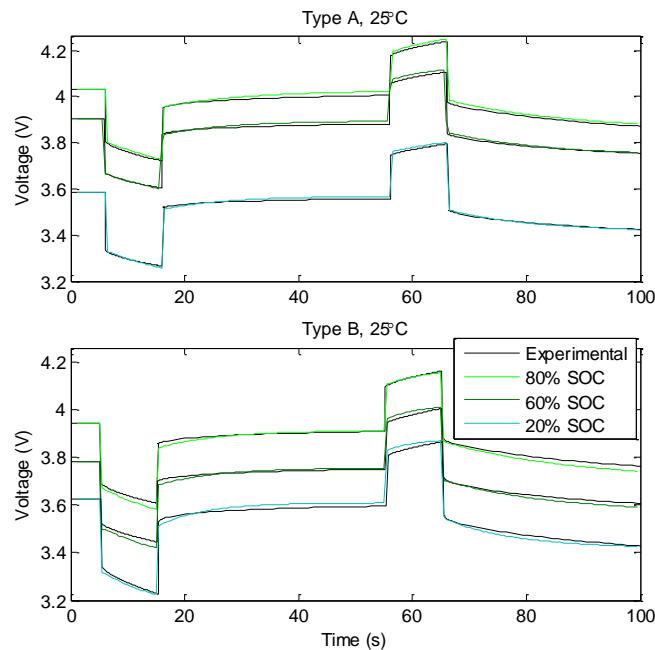


Figure 12: Model comparison for select pulses of the HPPC profile at 25°C, for cell types A and B.

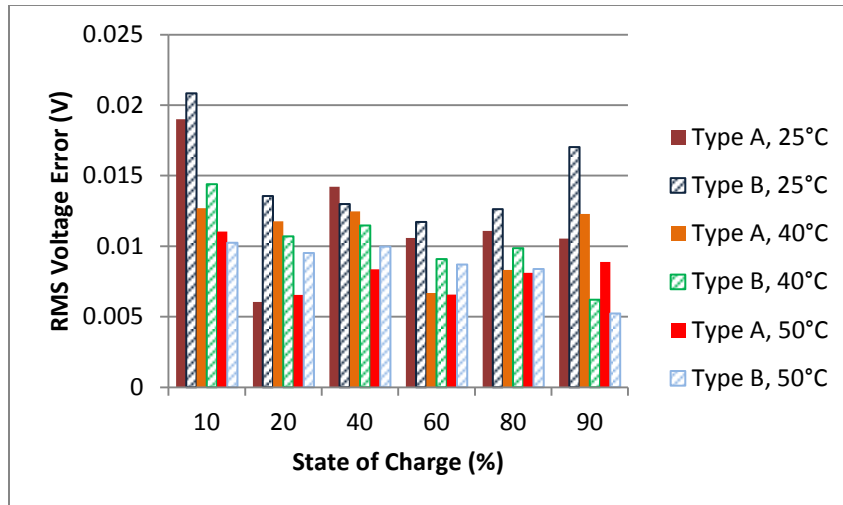


Figure 13: Root mean squared (RMS) voltage error between model and experiment for each cell type, at each SOC and temperature.

3.3 Multi-Rate Capacity Test Validation

The multi-rate capacity test consists of charging the cells to 100% SOC, followed by a rest period to allow the cell to equilibrate thermally and electrochemically, and then applying a constant discharge current until the lower voltage limit is reached. The duration of this experiment is typically longer than the previously analyzed HPPC results, and therefore thermal effects become more prominent. A comparison of the distributed model with the implemented SOC shift to experimental capacity tests is shown in **Fig. 14** and summarized in **Fig. 15**. The cell temperature for the model shown below represents an average temperature over the entire cell.

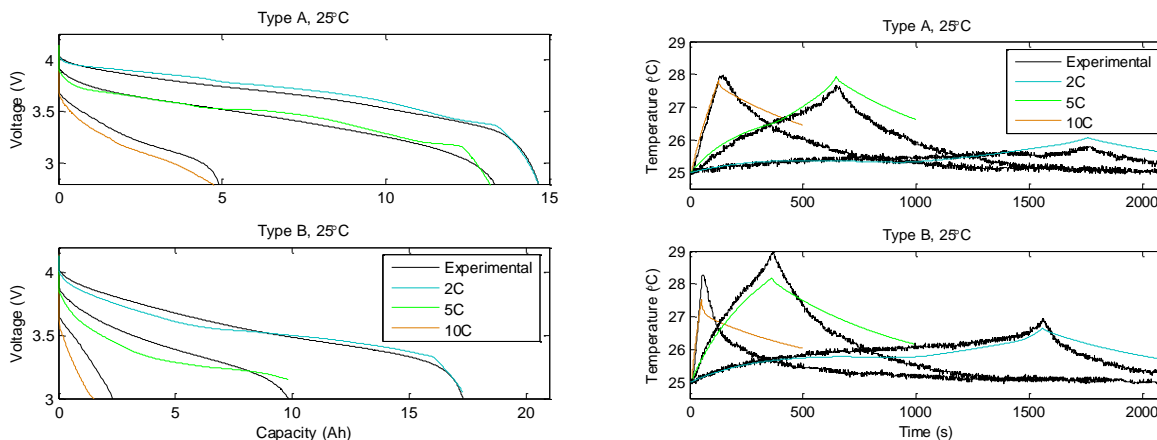


Figure 14: Model voltage and temperature comparison for select operating conditions.

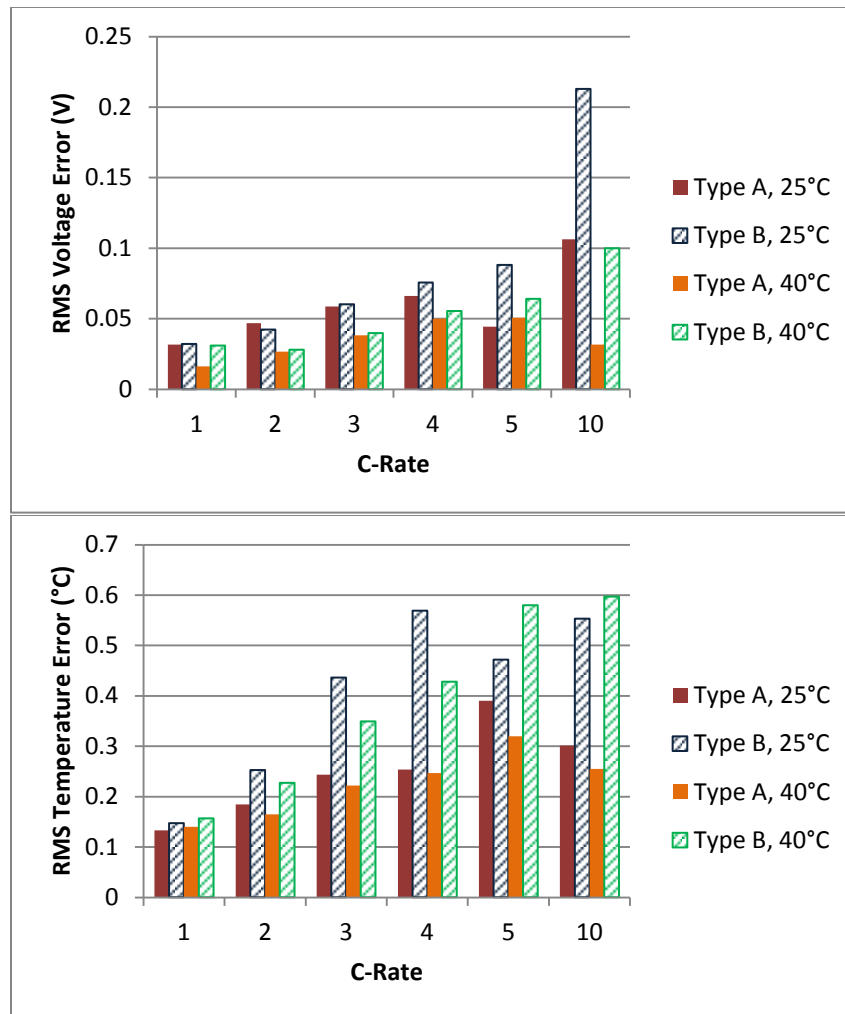


Figure 15: Voltage and average temperature RMS error between model and experiment for each cell type, at each operating condition.

4 Conclusion

A circuit based model has recently been added to LS-DYNA to simulate battery cells under different circumstances. The model can easily be coupled with external resistances, voltage and current sources, to connect the cell with its external environment. The additional data specific to the model can be visualized in LS-PrePost. The model is available in serial and MPP. The model gives good results for cells under normal use, and facilitates the analysis of multi-physics phenomena resulting from abuse conditions. First examples with comparisons with experiments were given. More examples are given in Ref [12] in this conference.

References

- [1] G. Zhang, C. Shaffer, C.Y. Wang, C. Rahn, “In-Situ Measurement of Current Distribution in a Li-Ion Cell”, *J. Electrochem. Soc.*, 160 (4), A610 – A615 (2013).
- [2] W. Zhao, G. Luo, C.Y. Wang, “Effect of tab design on large-format Li-ion cell performance”, *J. Power Sources*, 257, 70 – 79 (2014).

- [3] R. Spotnitz, S. Hartridge, G. Damblanc, G. Yeduvaka, D. Schad, V. Gudimetla, J. Votteler, G. Poole, C. Lueth, C. Walchshofer, E. Oxenham, “Design and Simulation of Spirally-Wound, Lithium-Ion Cells”, *ECS Trans.*, 50 (26), 209 – 218 (2013).
- [4] X. Hu, S. Li, and H. Peng, “A comparative study of equivalent circuit models for Li-ion batteries”, *J. Power Sources*, 198, 359 – 367 (2012).
- [5] G. Plett, “Extended Kalman filtering for battery management systems of LiPB-based HEV battery packs: Part 2. Modeling and identification”, 134, 262 – 276 (2004).
- [6] S. Allu, S. Kalnaus, W. Elwasif, S. Simunovic, J.A. Turner, S. Pannala, *J. Power Sources*, 246 (2014), 876-886.
- [7] G.H. Kim, K. Smith, K.J. Lee, S. Santhanagopalan, A. Pesaran, “Multi-Domain Modeling of Lithium-Ion Batteries Encompassing Multi-Physics in Varied Length Scales”, *J. Electrochem. Soc.*, 158 (8), A955 – A969 (2011).
- [8] K.J. Lee, K. Smith, A. Pesaran, G.H. Kim, “Three dimensional thermal-, electrical-, and electrochemical-coupled model for cylindrical wound large format lithium-ion batteries”, *J. Power Sources*, 241, 20 – 32 (2013).
- [9] M. Guo, G.H. Kim, R. White, “A three-dimensional multi-physics model for a Li-ion battery”, *J. Power Sources*, 240, 80 – 94 (2013).
- [10] D. Simon, *Optimal State Estimation*, John Wiley & Sons, Inc., Hoboken, New Jersey, (2006).
- [11] P. L’Eplattenier, I. Çaldichoury, *LS-DYNA EM theory manual*, LSTC, (2012).
- [12] J. Marcicki, A. Bartlett, X.G. Yang, V. Mejia, M. Zhu, Y. Chen, P. L’Eplattenier, I. Çaldichoury, "Battery Abuse Case Study Analysis Using LS-DYNA," presented at the 14th International LS-DYNA Conference, 2016.

Acknowledgments

The Ford authors acknowledge that this work was supported by the Vehicle Technologies Office, Office of Energy Efficiency and Renewable Energy, U.S. Department of Energy under DOE Agreement DE-EE0007288.